JCTC Journal of Chemical Theory and Computation

Intrinsic Viscosity of Proteins and Platonic Solids by Boundary Element Methods

David K. Hahn and Sergio R. Aragon*

Department of Chemistry and Biochemistry, San Francisco State University, 1600 Holloway Ave., San Francisco, California 94132

Received February 15, 2006

Abstract: The boundary element (BE) method is used to implement a very precise computation of the intrinsic viscosity for rigid molecules of arbitrary shape. The formulation, included in our program BEST, is tested against the analytical Simha formula for ellipsoids of revolution, and the results are essentially numerically exact. Previously unavailable, very precise results for a series of Platonic solids are also presented. The formulation includes the optional determination of the center of viscosity; however, for globular proteins, the difference compared to the computation based on the centroid is insignificant. The main application is to a series of 30 proteins ranging in molecular weight from 12 to 465 kD. The computation starts from the crystal structure as obtained from the Protein Data Bank, and a hydration thickness of 1.1 Å obtained in previous work with BEST was used. The results (extrapolated to an infinite number of triangular boundary elements) for the proteins are separated into two groups: monomeric and multimeric proteins. The agreement with experimental measurements of the intrinsic viscosity in the case of monomeric proteins is excellent and within experimental error of 5%, demonstrating that the solution and crystal structure are hydrodynamically equivalent. However, for some multimeric proteins, we observe strong systematic deviations around −20%, which we interpret as a systematic deviation of the solution structure from the crystal structure. A possible description of the structural change is deduced by using simple ellipsoid model parameters. A method to obtain intrinsic viscosity values for proteins to 1−2% accuracy (better than experimental error) on the basis of a single BE computation (avoiding the need for an extrapolation on the number of surface triangles) is also presented.

I. Introduction

The intrinsic viscosity, $[\eta]$, is simply the initial fractional slope obtained when the solution viscosity, η, is plotted against the concentration, c:

$$[\eta] = \lim_{c\to 0} \frac{\eta - \eta_o}{\eta_o c} \tag{1}$$

where η_o is the viscosity of the pure solvent. Thus, $[\eta]$ reflects the increase in viscosity brought about by the addition of an infinitesimal amount of solute to a pure solvent. Measurement of $[\eta]$ provides a simple and inexpensive way of obtaining information about molecular shape in solution, allowing phenomena such as protein denaturation[1] and oligomerization[2] to be examined.

Accurate computation of $[\eta]$ for macromolecules requires microscopic detail in the representation of the molecular surface. To achieve microscopic detail, the surface may be modeled in one of two ways: by a collection of small spherical beads (the hydrodynamic bead model) or by an array of flat triangular platelets (the boundary element, BE, method). While the bead model is well-known and has been previously applied to the computation of $[\eta]$ for proteins,[3] the problem can be formulated exactly as an integral equation that can be solved more accurately and precisely by the BE method.

The BE treatment by Zhou[4] used an approximate expression for $[\eta]$ accurate to within 2% for ellipsoids with axial ratios between $^1/_4$ and 4. Its application to globular proteins

* Corresponding author fax: 415-338-2384; e-mail: aragons@sfsu.edu.

10.1021/ct600062y CCC: $33.50 © 2006 American Chemical Society
Published on Web 06/30/2006

showed that a molecular surface based on the X-ray crystal structure is needed to obtain a description of hydration consistent with experimental protein hydration levels.[5] Allison[6] has since derived an exact BE expression for the intrinsic viscosity of a particle of arbitrary charge, situated in an arbitrary shear field and charge distribution. An application of this expression to the viscosity of ellipsoids[7] achieved agreement to within 1.0% of the exact value for axial ratios between $^1/_{10}$ and 10, even though a small number of platelets (<1000) were used to represent the surface.

In a previous paper,[8] hereafter referred as I, a thorough study of the translational and rotational diffusion coefficients of 41 globular proteins was presented. In I, the accuracy of a precise implementation of the boundary element method was clearly demonstrated. In this paper, the accuracy of our implementation is demonstrated with regard to the intrinsic viscosity of ellipsoids, polyhedrons, and globular proteins. Because of the rigorous nature of its implementation, the method's accuracy is limited only by the faithfulness of the representation of the hydrodynamic surface. Thus, when the hydrodynamic surface is constructed from crystallographic data, significant disagreement with an intrinsic viscosity experiment is indicative of either a difference in conformation between the crystal and solution phases or experimental error.

II. Theory

The hydrodynamic resistance problem for a particle translating with velocity $\mathbf{v}(\mathbf{y})$ at point y in a quiescent fluid can be formulated exactly as an integral over the surface of the molecule:[9]

$$\mathbf{v}(\mathbf{y}) = \int_{S_p} \overleftrightarrow{\mathbf{T}}(\mathbf{x},\mathbf{y})\, \mathbf{f}(\mathbf{x})\, \mathrm{d}S_x \tag{2}$$

where $\mathbf{f}(\mathbf{x})$ is the stress force at point x on particle surface S_p that must be solved for and $\overleftrightarrow{\mathbf{T}}(\mathbf{x},\mathbf{y})$, the Oseen hydrodynamic interaction tensor, is expressed as

$$\overleftrightarrow{\mathbf{T}}(\mathbf{x},\mathbf{y}) = \frac{1}{8\pi\eta_o|\mathbf{x}-\mathbf{y}|}\left[\overleftrightarrow{\mathbf{I}} + \frac{(\mathbf{x}-\mathbf{y})(\mathbf{x}-\mathbf{y})}{|\mathbf{x}-\mathbf{y}|^2}\right] \tag{3}$$

An approximate solution to eq 2 may be obtained by converting it into a matrix equation. This is accomplished by discretizing the surface of the molecule into triangular boundary elements.[10] The key assumption is that the surface stress force has a constant value within each of the N boundary elements

$$\mathbf{v}(\mathbf{y}_k) = \sum_{j=1}^{N} \int_{\Delta_j} \overleftrightarrow{\mathbf{T}}(\mathbf{x},\mathbf{y})\, \mathrm{d}S_x\, \mathbf{f}_j \tag{4a}$$

$$= \sum_{j=1}^{N} \overleftrightarrow{\mathbf{G}}_{kj} \cdot \mathbf{f}_j \tag{4b}$$

where Δ_j signifies integration over boundary element j (a triangle in this work). The resulting system of equations may then be solved for $\mathbf{f}_j$ using standard algebraic techniques. To compute different transport properties, one selects appropriate flows that specify the particular form of $\mathbf{v}(\mathbf{y})$. For the intrinsic viscosity, one selects five elementary shear flows[6]

$$\mathbf{v}_o^{(l)}(\mathbf{y}) = \frac{1}{2}\mathbf{E}^{(l)}(\mathbf{y}-\mathbf{d}) \tag{5a}$$

where $\mathbf{d}$ is the center of viscosity (the point where the dissipation of energy is minimized) and

$$\mathbf{E}^{(1)} = \gamma(\mathbf{e}_1\mathbf{e}_2 + \mathbf{e}_2\mathbf{e}_1) \tag{5b}$$

$$\mathbf{E}^{(2)} = \gamma(\mathbf{e}_1\mathbf{e}_3 + \mathbf{e}_3\mathbf{e}_1) \tag{5c}$$

$$\mathbf{E}^{(3)} = \gamma(\mathbf{e}_2\mathbf{e}_3 + \mathbf{e}_3\mathbf{e}_2) \tag{5d}$$

$$\mathbf{E}^{(4)} = \gamma(\mathbf{e}_1\mathbf{e}_1 - \mathbf{e}_2\mathbf{e}_2) \tag{5e}$$

$$\mathbf{E}^{(5)} = \gamma(\mathbf{e}_1\mathbf{e}_1 - \mathbf{e}_3\mathbf{e}_3) \tag{5f}$$

with γ being the shear gradient and $\mathbf{e}_\alpha$ being a unit vector along axis α in the laboratory frame of reference.

For convenience, the intrinsic viscosity may be expressed as the ratio between a dimensionless function of particle shape known as the viscosity factor, ξ, and the density of the particle, that is, $[\eta] = \xi/\rho$. When the viscosity factor is formulated in terms of the boundary element method, one obtains

$$\xi = -\frac{1}{\eta_o\gamma V_p}\int_{S_p}(\mathbf{y}-\mathbf{d})_b\mathbf{f}_a\, \mathrm{d}S_x \tag{6}$$

where subscripts a and b denote vector components along the flow direction and the direction of greatest shear, respectively, and V_p is the volume of the particle. Discretizing the surface integral and then averaging over all orientations of the particle yields[6]

$$\xi = \frac{1}{5}(\xi_{12}^{(1)} + \xi_{13}^{(2)} + \xi_{23}^{(3)}) + \frac{1}{15}(\xi_{11}^{(4)} + \xi_{33}^{(4)} - 2\xi_{22}^{(4)} + \xi_{11}^{(5)} + \xi_{22}^{(5)} - 2\xi_{33}^{(5)}) \tag{7a}$$

where

$$\xi_{\alpha\beta}^{(k)} = -\frac{1}{2\eta_o\gamma V_p}\left[\sum_{j=1}^{N} A_j(\mathbf{y}_j-\mathbf{d})(\mathbf{e}_\alpha\mathbf{e}_\beta + \mathbf{e}_\beta\mathbf{e}_\alpha)\mathbf{f}_j^{(k)}\right] \tag{7b}$$

where the summation runs over the surface elements and superscript k represents the five elementary shear fields for which the viscosity factor is evaluated. In eq 7b, A_j is the area of boundary element j, the stress force of shear field k on surface element j is denoted $\mathbf{f}_j^{(k)}$, and $\mathbf{y}_j$ represents the incenter of triangle j in the lab reference frame. The incenter of a triangle is the center of a circle that is inscribed within the triangle, and it differs, in general, from the centroid.

III. Computational Method

The theory presented above has been implemented in a Fortran 90 routine for calculating the intrinsic viscosity of an uncharged, arbitrarily shaped particle and was added to BEST,[11] a hydrodynamics program based on the method of Youngren and Acrivos[10] for numerically solving the integral form of the Stokes equations. Preliminary calculations on

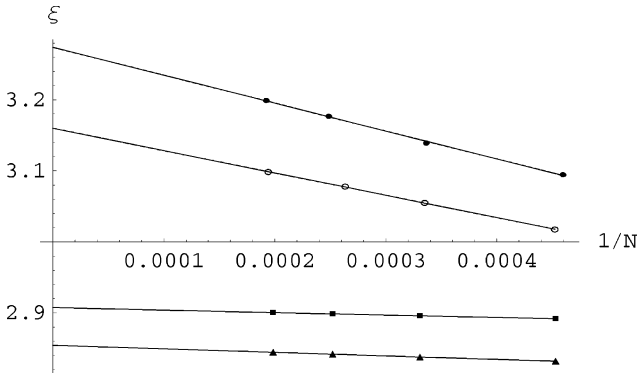

Figure 1. Graph of the viscosity factor as a function of the inverse triangle number, extrapolated to an infinite triangle number, for catalase (●), β-trypsin (○), an oblate ellipsoid of revolution with an axial ratio of 2 (▲), and a prolate ellipsoid of revolution with an axial ratio of $^1/_2$ (■). The protein data are fitted to a straight line, while the ellipsoid data are fitted to a quadratic line. A hydration layer thickness of $\delta = 1.1$ Å was used for calculating the protein viscosity factors.

ellipsoids showed that double precision accuracy would be needed in order to obtain results that correspond to experimental observations within the limits of experimental error. As discussed in some detail previously,[11] the accuracy of a BE calculation strongly depends on minimizing the error arising from the approximations used when integrating the Oseen tensor over the boundary elements of the tessellated surface. For this reason, double precision was assigned to all constants, variables, and operations in BEST, and the calculation of the Oseen tensor integral was increased to double precision accuracy using 21st order Gaussian quadrature. Double precision accuracy also eliminates round-off error from the BE calculation. Round-off error is manifested by a significant drop in the graph of the transport properties versus $1/N$ near $N = 2500$ when single precision accuracy is used.[11] No such drop is apparent in Figure 1.

Because $[\eta]$ is experimentally observed at the center of viscosity, the Fortran 90 routine computes the viscosity factor at this center or at the centroid of the molecule. The derivation of the center of viscosity within the framework of the BE method is provided in Appendix A, and all calculated values of $[\eta]$ reported herein were obtained at that center, unless otherwise noted. The program BEST calls LAPACK[12] routines including a set of basic linear algebra subroutines that have been hardware-optimized for the Opteron—the AMD core math library. The computation time for a given number of triangles varies from 2 to 20 min on dual processor AMD Opteron 248 servers with 4−16 GB of memory or a similar Itanium 2 workstation.

IV. Results and Discussion

We have performed several computations in order to demonstrate the accuracy and precision of the boundary element implementation of the intrinsic viscosity computation.

We first discuss the results as applied to ellipsoids of revolution for which analytical formulas are available for comparison. Then, we show new computations for a series

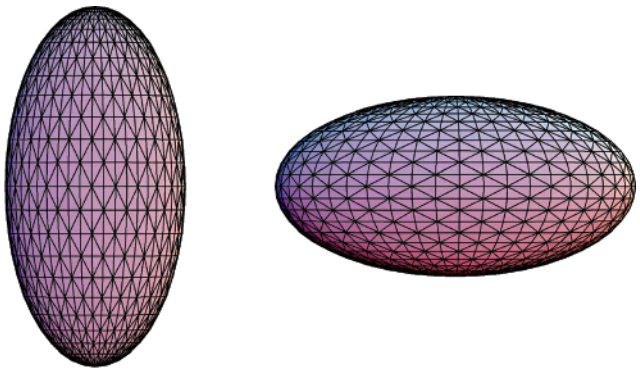

Figure 2. Triangulation of a prolate revolution ellipsoid, axial ratio $^1/_2$, and an oblate revolution ellipsoid, axial ratio 2, into 2208 platelets.

of Platonic solids to demonstrate that the presence of sharp corners presents no difficulty for the implementation. Finally, we present our computations for a set of globular proteins and find strong evidence for differences in solution structure compared to the crystal for some multimeric proteins.

IV.A. Ellipsoids of Revolution. The accuracy of our implementation of the BE method was determined through comparison with the exact analytical solution for the viscosity factor of an ellipsoid. To implement the BE method, the rigid ellipsoids were represented by a collection of flat, triangular surface elements (Figure 2). The tessellations for the ellipsoids and polygons discussed below were done by a program we constructed using Mathematica (Wolfram Research) because BEST requires a triangulation as input. The error in shape and surface area that arises when a curved surface is triangulated was removed by multiplying the 3×3 blocks represented by $\overleftrightarrow{\mathbf{G}}_{kj}$ in eq 4b by the appropriate correction factors.[11] The viscosity factor, $\xi(N)$, was computed with BEST over a range of values for N (specifically, $N =$ 2208, 3014, 3968, and 5040), and ξ was obtained from a polynomial least-squares fit of a plot of $\xi(N)$ versus $1/N$ extrapolated to an infinite triangle number. This is illustrated in Figure 1 for a prolate and oblate ellipsoid of revolution having an axial ratio of $p = {}^1/_2$ and 2, respectively. The extrapolation removes the discretization error, which arises because the surface stress force is approximated as a constant within each of the N boundary elements.

Table 1 compares the computed values of ξ to the exact values obtained from the Simha formula.[13] The error in the calculated value is below 0.01% for both the prolate and the oblate cases for all axial ratios less than or equal to 10. These results may be further improved by using an adaptive grid to triangulate the surface so that more triangles are situated in regions of high curvature and fewer are situated in regions of low curvature, demonstrating that our method is essentially numerically exact. The improvement compared to the previous work of Allison[7] is notable. However, the error in the present approach is 2 orders of magnitude smaller than the experimental uncertainty[14] in $[\eta]$, which is at least 1%, so improving our present values is not worthwhile. When applied to globular proteins, the accuracy of BEST is guaranteed if a well-triangulated, faithful representation of the hydrodynamic surface is employed.

Table 1. Viscosity Factor of Ellipsoids of Revolution and the Sphere

p	ξ^a	ξ(BEST)	% error
$^1/_{10}$	13.6343	13.6341	−0.0018
$^1/_9$	11.8043	11.8037	−0.0047
$^1/_8$	10.1026	10.1023	−0.0031
$^1/_7$	8.53274	8.53240	−0.0039
$^1/_6$	7.09876	7.09838	−0.0053
$^1/_5$	5.80621	5.80587	−0.0058
$^1/_4$	4.66332	4.66306	−0.0055
$^1/_3$	3.68488	3.68473	−0.0041
$^1/_2$	2.90761	2.90751	−0.0035
1	2.5	2.50004	0.0016
2	2.85437	2.85443	0.0019
3	3.43083	3.43080	−0.0001
4	4.05933	4.05940	0.0018
5	4.70821	4.70821	0.0000
6	5.36720	5.36720	0.0000
7	6.03194	6.03196	0.0003
8	6.70027	6.70083	0.0083
9	7.37099	7.37112	0.0018
10	8.04337	8.04359	0.0027

IV.B. Platonic Solids. The Platonic solids are of interest because their sharp corners provide a severe test of the robustness of the boundary element method implemented in this work. Both uniform and edge-enhanced triangulations of the polyhedron surface, Figure 3, were used to calculate

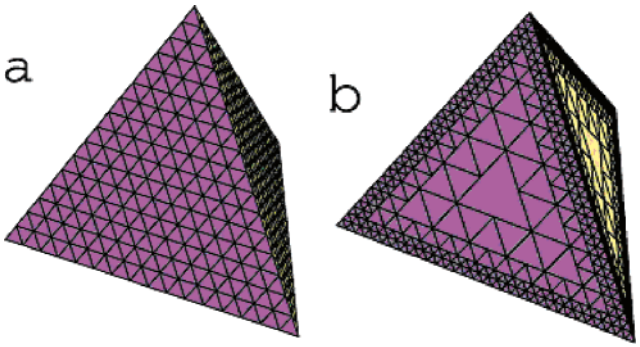

Figure 3. (a) Uniform triangulation of the tetrahedron into 1024 platelets. (b) Edge-enhanced triangulation of the tetrahedron into 1756 platelets.

ξ. The uniform triangulation tessellates the surface by repeatedly subdividing each triangular facet into four equilateral triangles. In this study, up to $N = 10\,000$ was used, requiring a machine with at least 8 GB of memory. The edge-enhanced tessellation requires at least one initial uniform triangulation in order to obtain interior and exterior triangles on each facet, whereupon only the exterior triangles are subdivided in each subsequent refinement. For polyhedrons composed of *n*-polygonal facets rather than triangular facets, such as the cube and dodecahedron, an initial tessellation of each facet into *n* triangles is also required. A polynomial least-squares fit of a plot of $\xi(N)$ as a function of $1/N$ yielded ξ from the extrapolation to infinite *N*. The edge-enhanced tessellation is expected to produce more accurate results because this kind of tessellation allows one to define the corners and edges more precisely with a given number of data points at large values of *N*, and these are the regions where the surface stress varies more rapidly.

Table 2. Viscosity Factor of Platonic Solids

		ξ (BEST)	
structure	S/V^a	uniform	edged
tetrahedron	9.0000	4.172	4.210
cube	5.1962	3.096	3.118[b]
octahedron	5.1962	2.996	3.016
dodecahedron	3.7752	2.683	2.691
icosahedron	3.3887	2.632	2.636

[a] Surface-to-volume ratio. [b] Estimated from the tetrahedron behavior.

Use of the edge-enhanced tessellation is justified by the larger variation in the surface stress force near the edges and vertexes of each facet, which requires a greater density of triangles; the surface stress force is nearly constant toward the center of each facet. These circumstances may be inferred from a comparison of the results in Table 2. For example, the difference between the edged and uniform results is largest for the tetrahedron. Because this is the Platonic solid with the most prominent vertexes, it has the largest variation in $\mathbf{f}(\mathbf{x})$ on its surface, and the result from the uniform tessellation has the largest error. Conversely, the icosahedron has the least prominent vertexes of all of the Platonic solids, and the difference between the edged and uniform results is the smallest. The extrapolations versus $1/N$ for the polyhedra show linear behavior as in Figure 1, with no significant differences between the uniform and edge-enhanced tessellations. (The edge-enhanced tessellation for the surface of the cube leads to linear dependence in $[\overleftrightarrow{\mathbf{G}}_{kj}]$, so that the value in Table 2 is estimated from the behavior of the octahedron.)

Polyhedra have biological and chemical significance; HIV-1 and many other small viruses have icosahedral symmetry,[15] for example, and of course C_{60} is a truncated icosahedron. It does not appear that the viscosity factor of any polyhedron has been obtained previously, in either numerical or analytical form, so these very accurate values are new. (The viscosity of structures composed of beads situated at the vertexes of a polyhedron has been determined,[16] but this is not an appropriate comparison to the present results.) However, the size of ξ should at least reflect the surface-to-volume ratio, *S*/*V*, of a structure. A decrease in *S*/*V*, for example, causes a decrease in the amount of friction generated with the surrounding fluid and a concomitant decrease in ξ. Table 2 shows that BEST does in fact predict values for ξ that are consistent with the *S*/*V* of the polyhedrons. In addition, the value of ξ appropriately converges on 2.5, the exact value for a sphere,[17] which has the smallest possible surface-to-volume ratio. The estimated uncertainty in the edged values of the viscosity factor is 0.03%, except for the estimated value of the cube for which the uncertainty is no more than 0.1%. All of the viscosity factors presented below were obtained from extrapolations versus $1/N$. The viscosity factor was also calculated for two nonplatonic polyhedrons. For the truncated icosahedron, we obtained $\xi = 2.546$, and for the icosidodecahedron, $\xi = 2.588$.

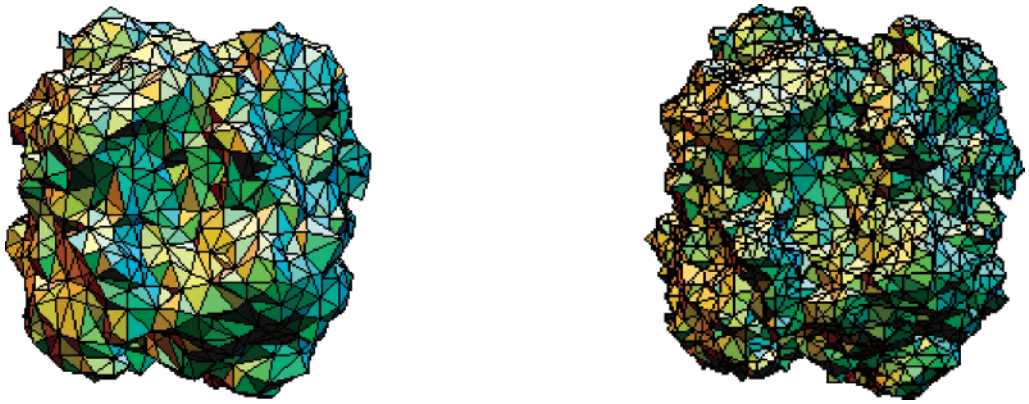

Figure 4. Surface of catalase (4BLC) triangulated with Msroll and processed with Coalesce to yield 2248 triangles (left) and 4154 triangles (right).

IV.C. Proteins. To extend the study to proteins, molecular surfaces were constructed from crystallographic data using MSROLL.[18] Coalesce,[11] which reduces N by merging small and slender triangles, was then applied to make the triangulations more suitable for the BE method. Figure 4 shows the triangulated surface for the large protein catalase. Hydration was modeled by uniformly increasing the van der Waals radius of all of the atoms in the PDB file (the inflation model of solvation) before creating the molecular surface. The optimum value of the hydration layer thickness, $\delta = 1.1 \pm 0.1$ Å, was determined in I by minimizing the disagreement between the computed and experimental values of the translational diffusion coefficient (D_t) for a set of four well-studied proteins, namely, ribonuclease, lysozyme, myoglobin, and chymotrypsinogen a.

To optimize δ, $D_t(N)$ and $[\eta(N)]$ were computed in the region where N is large enough for the plots against $1/N$ to be linear. The transport properties were then obtained from a straight-line fit extrapolated to an infinite triangle number.

The location of the linear region depends on how the molecular surface is constructed. More precisely, it is sensitive to the number of triangles eliminated by Coalesce, because the surface roughness decreases as the number of eliminated triangles increases, and this affects the curvature in a plot of the transport properties against $1/N$.

In turn, the number of eliminated triangles depends on the number of triangles in the molecular surface obtained from MSROLL, which is controlled by a fineness parameter.

For most of the proteins in this study, the MSROLL molecular surface contained at least 20 000 triangles, and the region of linearity extended down to approximately $N = 2000$ after processing by Coalesce. This is demonstrated in Figure 1, which shows the linear fit to the plot of $\xi(N)$ against $1/N$ using data obtained for β-trypsin and catalase.

Processing the MSROLL triangulation with Coalesce also reduces the amount of scatter in a plot of the transport properties against $1/N$. Combined with the high precision of BEST, there results an excellent straight-line fit for small proteins such as β-trypsin, as Figure 2 shows. The scatter tends to increase with increasing particle size, but even for β-galactosidase, the largest protein in the data set, there is only a 0.1% statistical error on the intercept, and a small number of points are needed for confidence. (For very large particles, the data set may contain a data point with a discordant value. In such instances, a "Q test" should be performed on the residuals of a linear regression analysis of the data to determine whether the suspect value should be retained.[19] Data points that do not pass the Q test can be discarded.)

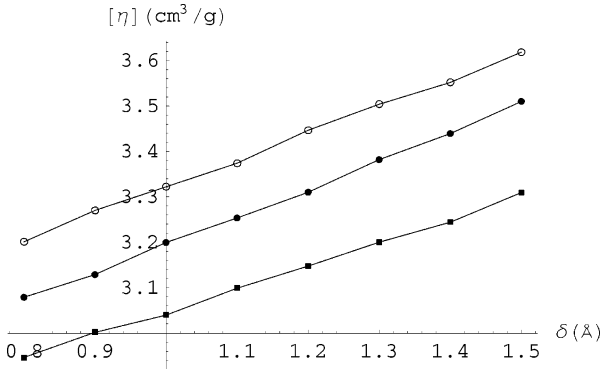

Figure 5. Graph of the intrinsic viscosity as a function of the hydration layer thickness for myoglobin (○), lysozyme (●), and chymotrypsinogen (■).

The transport properties are smooth functions of δ when $[\eta(N)]$ values are calculated in the linear region, as Figure 5 shows. $[\eta]$ varies by approximately 0.06 cm^3g^{-1} for every 0.1 Å increase in δ. An optimum value of 1.1 Å is also obtained for δ when minimizing the discrepancy of $[\eta]$ for a small test set of proteins, but with a larger uncertainty, compared to the value obtained in I. Thus, we find that a single value of the hydration thickness is suitable for all transport properties, including the intrinsic viscosity. Zhou[5] obtained a smaller hydration layer thickness, 0.9 Å, which we attribute to differences in tessellation methods. While MSROLL uses spherical, toroid, and saddle regions to represent the molecular surface, Zhou used only spherical polygons, which resulted in undersized excluded molecular volumes. The smaller hydration layer obtained by Zhou compensates for this because it results in a rougher molecular surface and, therefore, a larger viscosity factor, allowing the calculated and experimental values of $[\eta]$ to match each other.

Table 3 compares calculated and literature values of $[\eta]$ and D_t for 30 globular proteins. For each protein, only crystallographic, viscometric, and diffusion data obtained

Table 3. Intrinsic Viscosity and Translational Diffusion Coefficient of Native Proteins

protein	s[a]	mass (kDa)	$[\eta]$ (cm^3/g)				D_t (10^{-7}cm^2/s)			
			calcd	exptl	ref	Δ^b	calcd	exptl	ref	Δ^b
cytochrome C (1HRC)	1	12.4	3.07	2.74	21	13	11.63	11.1−12.1	22−25	0
ribonuclease A (7RSA)[c]	1	13.7	3.52	3.30, 3.50	26, 27	3	10.84	10.68	28	2
α-lactalbumin (1HFX)	1	14.2	3.41	3.01, 3.4	29, 30	6	10.84	10.57, 10.6	31, 32	2
lysozyme (2CDS)	1	14.3	3.22	2.66−3.00	33−37	12	11.04	10.6, 11.2	38, 36	1
myoglobin (1MBO)	1	17.2	3.37	3.25	39	2	10.24	10.4, 10.5	40, 41	−2
soyb. tryp. inhib. (1AVU)	1	20.1	3.18	2.8	42	14	9.88	9.8	43	1
β-trypsin (1TPO)	1	23.3	3.08	3.1	44	0	9.50	9.3	45	2
trypsinogen (1TGN)	1	24.0	3.00	2.96	46	1	9.49	9.68	47	−2
α-chymotrypsin (4CHA)	1	25.2	3.25	3.00	44, 48	8	9.08	10.20	48	−11
chymotrypsinog. A (2CGA)	1	25.7	3.20	2.5, 3.13	49, 50	4	9.16	9.23	51	−1
carbonic anhyd. B (2CAB)	1	28.8	3.07	2.76, 3.2, 3.7	52, 37, 53	−5	8.84	8.89	52	−1
Zn-α2-glycoprotein (1ZAG)	1	32.6	4.88	5.0	54	−2	7.32	6.5	54	12
pepsin (4PEP)	1	34.5	3.33	3.09, 3.35	55, 56	3	8.10	8.01, 8.71	57, 56	−3
G-ADP actin (1J6Z)	1	43.0	3.56	3.7	58	−3	7.39	7.15, 7.88	59, 60	−2
Taka-amylase A (6TAA)	1	52.5	3.15	3.3	61	−3	7.22	7.37	62	−2
human serum Alb. (1AO6)	1	66.5	4.12	3.9, 4.2, 4.73	63−65	−3	6.07	5.9, 6.1, 6.3	66, 64, 67	−1
ovotransferrin (1OVT)	1	76.0	3.83	3.8	68	0	6.03	5.9	69	2
lactotransferrin (1LFG)	1	77.1	3.97	4.0	70	0	5.87	5.6	71	5
superoxide dismu. (2SOD)	2	32.5	3.57	3.3	72	9	8.10	8.27	72	−2
β-lactoglobulin (1BEB)[c]	2	36.7	3.65	3.4−4.2	73−76, 37	−5	7.74	7.3	77, 31	5
α-chymotrypsin (4CHA)	2	50.4	3.31	4.1, 4.25	78, 79	−21	7.17	7.1, 7.40	80, 79	−1
concanavalin (1GKB)	2	51.4	3.95	4.1	81	−2	6.72	6.2	82	8
triosephos. isom. (8TIM)	2	53.2	3.59	3.75	83	−4	6.88	6.76	83	2
ricin (2AAI)	2	61.5	3.33	2.96	84	13	6.61	6.0	85	10
oxyhemoglobin A (1HHO)	4	63.2	2.89	2.77	20	4	7.03	6.78	86	4
alkaline phosphat. (1ALK)	2	94.6	3.09	3.4	87	−7	5.96	5.7	88	4
citrate synthase (1CTS)	2	98.0	3.20	3.95	89	−20	5.82	5.8	89	0
inorganic pyrophos. (1FAJ)	6	117.3	2.93	4.0	90	−28	5.62	5.7	90	−2
aldolase (1ADO)	4	157.1	3.84	3.4, 4.0, 4.04	91−93	0	4.66	4.29−4.8	94−97	4
catalase (4BLC)	4	235.7	3.08	3.9	98, 99	−21	4.49	4.1	100, 101	10
β-galactosidase (1BGL)	4	465.8	3.84	3.78	102	2	3.26	3.13	102	4

[a] Number of subunits. [b] The percent difference between the calculated and experimental value determined from the average of the experimental values. [c] Heavy atoms only.

from the same species are considered. (A possible exception exists for trypsin and pepsin, for which the source of the protein in the viscosity experiment was not specified.) This precaution is taken because $[\eta]$ may depend on the source of the protein, even if that protein's molecular weight does not significantly differ from one strain to the next.[20]

The present computational model for investigating protein viscosity contains three assumptions: the crystal- and solution-phase geometries of the protein are identical, the thickness of the hydration layer is uniform, and the hydration layer is smooth on the measurement time scale. In light of the accuracy demonstrated in Table 1, any significant discrepancy between theory and measurement may be attributed to either a failure of one of these assumptions or experimental error.

For almost all of the monomeric proteins in Table 3, the assumptions of the computational model appear to be valid, as it is possible to find at least one value for $[\eta]$ from the literature that is within 5% of the calculated value. For several of the oligomeric proteins, however, the value of $[\eta]$ is significantly underestimated by the calculation. A possible explanation is that the assumption regarding the geometry is not valid for these proteins. The subunits of oligomeric proteins are typically bound together by noncovalent forces that may weaken in solution, resulting in a greater separation compared to the crystal phase, a more elongated shape, and a larger value of $[\eta]$. Support for this hypothesis is particularly apparent in the comparison between the results for the α-chymotrypsin monomer and dimer entries in Table 3. (A single chain from the PDB file 4CHA was used to represent the monomer geometry.) The computed value of the monomer intrinsic viscosity exceeds the measured value by only 8%, while the computed value of the dimer intrinsic viscosity undershoots the measured values by about 20%.

A closer examination of the results in Table 3 reveals that four multi-subunit proteins have large underestimations of $[\eta]$ that generally occur for oligomers with a weak noncovalent contact between subunits in solution. The dimers of α-chymotrypsin[103] and citrate synthase,[104] for example, undergo a reversible equilibrium between the associated and dissociated species, which is typical of oligomeric proteins with weakly bound subunits, and the intrinsic viscosity of both of these proteins is underestimated by about 20%. Hexameric inorganic pyrophosphatase of *Escherichia coli* also appears to have a weak noncovalent interchain bond; under mildly acidic conditions, it dissociates into two trimers.[105] The intrinsic viscosity for this protein is underestimated by nearly 30%.

For catalase and oxyhemoglobin, however, the strength of the subunit contact does not correlate with the error in $[\eta]$. Tetrameric catalase is stable over a wide range of pH values,[98] while $[\eta]$ is underestimated by 19% for this protein. Conversely, the physicochemical behavior of oxyhemoglobin does not suggest strong subunit contacts,[111] while the calculated value of $[\eta]$ for this protein is accurate to within the limits of experimental uncertainty. Nevertheless, the precision of the computations is strong evidence for discrepancies in the solution and crystal structure for the four proteins whose intrinsic viscosity is underestimated by 20% or more. It is also possible that there is some difference in structure in going to solution for the extra cases where the discrepancy is greater than 10%, as in the cases of ricin among the oligomeric proteins and cytochrome C and soybean tripsin inhibitor among the monomeric proteins. The case of lysozyme is unclear because the experimental values have such a wide range.

A much smaller discrepancy in $[\eta]$ is obtained for most of the oligomeric proteins with a strong noncovalent interaction between subunits. Superoxide dismutase,[106] aldolase,[107] concanavalin,[108] alkaline phosphatase,[109] and triosephosphate isomerase[110] all have a strong solution-phase noncovalent contact between subunits, on the basis of physicochemical studies, and the computed intrinsic viscosity for these proteins agrees with experimental results to within 10%. The small discrepancy in $[\eta]$ for oxyhemoglobin conforms to the quaternary structure of carbonmonoxy hemoglobin in solution, which has been characterized by NMR measurements as an intermediate between two known crystal structures.[112] These crystal structures differ by a 13.3° rotation of two subunits (an $\alpha\beta$ dimer) relative to the other two, with little change in the center of mass separation between the subunits.[113] Ricin is the only oligomeric protein in the data set with an interchain disulfide bond.[114] The positive error in the calculated value for the intrinsic viscosity of this protein is partially due to this covalent interaction, yet it too may have a change in conformation, as described below.

IV.D. Qualitative Geometry Changes in Oligomeric Proteins. Our precise treatment of the intrinsic viscosity demonstrates that an accurate description of the real shape of a macromolecule is necessary to obtain reasonable quantitative accuracy. Nevertheless, if we desire only qualitative information, then an ellipsoidal model could be used because it is simple enough to be analytically solved. This does not imply that we believe ellipsoidal models are useful for anything other than a qualitative exploration of shape effects. A qualitative description of the difference between the crystal structure and the solution-phase geometry may be determined from data in Table 3 by modeling the proteins as ellipsoids of revolution. From the relation $[\eta] \propto V_p\, \xi(\rho)$ for an ellipsoid of axial ratio ρ and volume V_p and having a Simha factor of $\xi(\rho)$, one obtains

$$\xi(\rho') = (1 + q)(V_p/V_p')\, \xi(\rho) \tag{8}$$

where the prime denotes a measured value and unprimed denotes a calculated value and where q is the fractional error in $\xi(\rho)$. Similarly, $D_t \propto G(\rho)/a$ for an ellipsoid of length a having a shape factor of $G(\rho)$, so that

$$G(\rho') = (1 - r)(a'/a)\, G(\rho) \tag{9}$$

where r is the fractional error in $G(\rho)$. Multiplying $\xi(\rho')$ by $G(\rho')$ and assuming $V_p/V_p' = a/a'$, one obtains

$$\xi(\rho')\, G(\rho') = (1 + q)(1 - r)\, \xi(\rho)\, G(\rho) \tag{10}$$

which may then be solved for ρ'. The geometry change is then deduced from the change in ρ, a, and V_p consistent with the signs of p and q. For example, the α-chymotrypsin dimer has a computed viscosity factor corresponding to an ellipsoid with $\rho = 0.38$, while $q = -0.20$ and $r = 0.03$ from Table 3, so that the solution of eq 10 yields $\rho' = 0.32$. The comparison between ρ and ρ' indicates that the protein is less spherical in solution. The behavior of $V_p\, \xi(\rho)$ and $G(\rho)/a$ as a function of ρ then dictates that the protein must also expand, in addition to becoming less spherical, to satisfy the condition imposed by the values of q and r.

Table 4. Qualitative Solution-Phase Geometry Change

protein	Δ $[\eta]$	Δ D_t	r	ρ¢	inference
cytochrome C[a]	>0	0	0.45	0.51	shrink and more spherical
lysozyme	>0	0	0.40	0.43	shrink and more spherical
soybean trypsin inhibitor	>0	0	0.36	0.42	shrink and more spherical
ricin	>0	>0	0.37	0.46	more spherical
α-chymotrypsin	<0	0	0.38	0.32	expand and less spherical
citrate synthase	<0	0	0.39	0.34	expand and less spherical
inorganic pyrophosphatase	<0	0	0.45	0.36	expand and less spherical
catalase	<0	>0	2.9	2.4	expand and/or less spherical

[a] See text.

An oblate model was used for catalase, and a prolate model was used for the remaining proteins (by examination of their rotational diffusion tensors in paper I). Table 4 provides a summary of the geometry changes for each of the five cases encountered in the present set of proteins. Cytochrome C is an interesting case. Along with lysozyme and soybean trypsin inhibitor, they are the only 3 of 18 monomeric proteins that show a significant positive discrepancy. As mentioned previously, the experimental data for lysozyme have a broad range, so the discrepancy could be as little as 7%, so no change in going to solution may be present. Cytochrome C, unlike the other two, has a very asymmetric rotational diffusion tensor and cannot be represented as an ellipsoid of revolution. The crystal structure has "three major and two minor helical elements interconnected by strands of polypeptide chain and folded into a roughly globular shape within which a (hydrophobic) heme pocket is formed."[115] If one insists on the assignment of a prolate shape, then the discrepancies predict that the protein will become more spherical in solution, as shown in Table 5. However, if we consider it to be oblate, we conclude the opposite: it becomes less spherical ($\rho = 2.83$ and $\rho' = 3.59$). The ellipsoid model does not work even qualitatively for this protein.

The ellipsoid model predicts that ricin becomes more spherical in solution without undergoing a change in size, suggesting torsional motion around the interchain disulfide

bond without a change in the distance between the subunits. In addition to the disulfide bond, a strong noncovalent interaction is known to exist between ricin's A and B chains,[116] so it is surprising that this protein shows a moderate positive discrepancy in both the intrinsic viscosity and the translational diffusion coefficient.

It is noteworthy that the crystal- and solution-phase geometries may differ and yet the translational diffusion coefficients may not show a large change. For the majority of the oligomers, the error in D_t is positive, larger than that of the monomers, and smaller than that of $[\eta]$. These results are anticipated from a simple ellipsoid model; for an ellipsoid of length a and axial ratio $\rho = b/a$, $D_t \propto G(\rho)/a$. Because the shape function $G(\rho)$ is more slowly varying than a in the region relevant to globular proteins ($\rho \approx {}^1/_2$), a positive error in D_t is predicted by the ellipsoid model if a is too small. However, the errors in $G(\rho)$ and a at least partially cancel each other out when D_t is calculated. Because $[\eta] \propto V_p\, \xi(\rho)$ for an ellipsoid of volume V_p, any error in V_p will be amplified by the accompanying error in $\xi(\rho)$, so that a larger error arises when $[\eta]$ is calculated.

V. Computational Shortcuts

Two aspects of the very precise method lead to large computer memory requirements, and large computation times. Because the solution of a linear system is an N^3 process, using large numbers of triangles slows the computation considerably, while computing the center of viscosity requires the even more time-consuming (and doubling the memory requirement) explicit inverse matrix computation. In this section, we demonstrate that both of these problems can be circumvented. First, we show that the centroid is quite sufficient so that the center of viscosity is not required for protein computations. Second, we obtain a simple linear extrapolation equation that allows the computation of the viscosity factor from a single BE calculation at a moderate number of triangles, eliminating the need to compute at many values of the triangle number and extrapolating to an infinite number of triangles.

V.A. Intrinsic Viscosity Values from a Single BE Computation. For a machine with only 1 GB of RAM, the maximum number of triangles that memory storage permits is around 3000. The calculations detailed above have used machines with up to 16 GB of RAM. Thus, the question arises, can we obtain a useful transport property without requiring extrapolations including very large numbers of triangles? The data presented in Table 4 demonstrate that we can give an affirmative answer to the previous question. The slope of the extrapolations as a function of $1/N$ is not large, and the slope divided by the intercept does not vary widely across the protein data set. Thus, it is possible to estimate the extrapolated value to an infinite number of triangles by using Q, the average slope/intercept, over a protein data set. This implies that, given the value Q for each property, one can perform a single calculation with 2000−3000 triangles and obtain a value for a viscosity factor with a statistical error of about 1−2%. This is 2 to 4 times worse than the statistical error of the accurate extrapolations but still much better than the experimental error. Using regression data from plots of $[\eta(N)]$ versus $1/N$ for a set of proteins, an average slope/intercept, Q, is obtained, and the intrinsic viscosity can be quickly calculated as

$$[\eta] = [\eta(N)]/(1 + Q/N) \tag{11}$$

For the set of 30 proteins in Table 3, $Q = -102.31$. Table 5 shows the value of $[\eta(N)]$ at the given value of N, the extrapolation using eq 11, and its error for each of the 30 proteins. Agreement between the formula and the accurate extrapolated value has a standard deviation just over 1% and is at worst 4%. Because the typical uncertainty in a measurement of $[\eta]$ is 5%, eq 11 may be used with no significant loss in accuracy or precision with the consequent savings in effort and lesser hardware requirements. More precise values can be obtained from a single BE computation if N is larger than 3000.

Table 5. Protein Intrinsic Viscosity from a Single BE Computation

protein	N	$[\eta(N)]$	$[\eta]$	% error
cytochrome C (1HRC)	2316	3.029	3.168	3.21
ribonuclease A (7RSA)	2560	3.394	3.535	0.43
lysozyme (2CDS)	2580	3.140	3.270	1.54
α-lactalbumin (1HFX)	2558	3.245	3.380	−0.88
myoglobin (1MBO)	2774	3.230	3.354	−0.47
soybean trypsin inhibitor (1AVU)	2900	3.032	3.143	−1.18
β-trypsin (1TPO)	2428	2.957	3.087	0.22
trypsinogen (1TGN)	2678	2.890	3.005	0.16
α-chymotrypsin (4CHA)	2566	3.081	3.209	−1.25
chymotrypsinogen A (2CGA)	2214	3.080	3.229	0.90
carbonic anhydrase B (2CAB)	2500	2.959	3.086	0.51
Zn-α2-glycoprotein (1ZAG)	2170	4.624	4.853	−0.56
pepsin (4PEP)	2600	3.201	3.332	0.07
G-actin (1J6Z)	2218	3.369	3.532	−0.79
Taka-amylase (6TAA)	2396	3.018	3.152	0.07
human serum albumin (1AO6)	2630	3.874	4.031	−2.16
ovotransferrin (1OVT)	2426	3.644	3.805	−0.66
lactoferrin (1H76)	2316	3.757	3.930	−1.00
superoxide dismutase (2SOD)	2472	3.426	3.574	0.12
β-lactoglobulin (1BEB)	2206	3.458	3.626	−0.65
α-chymotrypsin (4CHA, dimer)	2670	3.150	3.276	−1.03
concanavalin (1GKB)	2180	3.774	3.960	0.25
triosephosphate isomerase (8TIM)	2672	3.422	3.558	−0.89
ricin (2AAI)	2204	3.294	3.454	3.73
oxyhemoglobin A (1HHO)	2712	2.708	2.814	−2.61
alkaline phosphatase (1ALK)	2724	3.074	3.194	3.36
citrate synthase (1CTS)	2812	3.123	3.241	1.28
inorganic pyrophosphatase (1FAJ)	2296	2.882	3.016	2.94
aldolase (1ADO)	2466	3.693	3.852	0.32
catalase (4BLC)	2994	2.858	2.959	−3.93

V.B. Consequences of Calculating [η(N)] at the Centroid. The calculation of $[\eta(N)]$ may be expedited by performing it at the centroid instead of the center of viscosity. Evaluation of the center of viscosity requires explicit inversion of the Oseen tensor matrix, which is the most time-consuming step in the calculation of $[\eta(N)]$. Neglecting this calculation allows the direct solution of eq 4—a much faster alternative that does not require storage of the inverse matrix. Because globular proteins are roughly spherical or ellipsoidal, the centroid should nearly coincide with the center of viscosity,

and this is indeed the case for all of the proteins in this study. Typically, the computed distance between the center of viscosity and the centroid is less than 0.7 Å and tends to decrease with increasing N. For citrate synthase (1CTS), the distance between the viscosity center and centroid is unusually large, being 1.1 Å for $N = 2108$. However, only a 0.08% difference in $[\eta(N)]$ was found to arise when the calculation was performed at the centroid rather than the viscosity center. The difference in CPU time for the two calculations was 474 s on an AMD Opteron 64-bit processor. Our program BEST provides a flag to compute the viscosity factor at either center.

VI. Summary and Conclusions

We have implemented a very accurate boundary element method to determine the intrinsic viscosity of arbitrarily shaped objects. Our formulation is in numerically exact agreement with the Simha formula for ellipsoids of revolution. We are able to calculate high precision values of the intrinsic viscosity for sharp-cornered polyhedra, some of which are representative of viral shapes. In the application to proteins, we have found that the same uniform hydration layer thickness of 1.1 Å that was successfully used to model diffusion tensors in I also works for the intrinsic viscosity. Thus, a uniform hydration layer provides an excellent hydrodynamic model for the accurate computation of all transport properties of proteins. Because the intrinsic viscosity is a function of shape, independent of the size of an object, our study also allows us to compare the molecular shape in the crystal and in solution. For almost all monomeric proteins, the method agrees within experimental error with the measured intrinsic viscosities of proteins, demonstrating that the conformation in the crystal and that in solution are hydrodynamically indistinguishable.

For several multi-subunit proteins, the computational model has sufficient accuracy to strongly suggest that the crystalline- and solution-phase geometries are different. Most of the proteins whose subunits are bound together by weak noncovalent forces show a discrepancy consistent with a shape change in going to solution from the crystal. We have proposed a simple qualitative model to understand what type of shape change could account for the observed differences. A characterization of the possible shape changes is presently being pursued in our laboratory using implicit solvent molecular modeling with Amber 8 with encouraging initial results. That work will be reported elsewhere. Finally, we have also proposed a simple equation that permits the computation of the intrinsic viscosity to within 2% using a single BE computation, making these calculations possible in readily available computer hardware.

Note Added in Proof: Prof. J. Michael Schurr made us aware that the crystal structure may fail to include all the residues of a protein. This is actually the case for one third of the proteins studied here. However, the percentage of missing residues is small, typically around 2%, so that the conclusions of the paper are not affected.

Acknowledgment. This research was supported through a grant from the National Institutes of Health, MBRS SCORE Program, Grant S06 GM52588 to S.A.

Appendix A: Derivation of the Center of Viscosity

The center of viscosity is obtained by applying the condition to eq 7a and solving for $\mathbf{d}$. The dependence of $\mathbf{f}_j^{(l)}$ on $\mathbf{d}$

$$\frac{\partial \xi}{\partial \mathbf{d}} = 0 \tag{A1}$$

must first be made explicit, that is,

$$\mathbf{f}_{\mathrm{j}}^{(\mathrm{l})} = \mathbf{U}_{\alpha\beta_j}{}^{-1} \times \mathbf{y}_j + \mathbf{d} \times \mathbf{U}_{\alpha\beta_j}{}^{-1} \tag{A2a}$$

$$= \mathbf{g}_{\alpha_j}^{(l)} + \mathbf{d} \times \mathbf{h}_{\alpha\beta_j}^{(l)} \tag{A2b}$$

where $\mathbf{U}_{\alpha\beta}$ is a matrix element of the Oseen tensor integral. Substituting eq A2b into eq 7a and performing the multiplication between the unit vectors then gives

$$\begin{aligned}\xi = \frac{1}{15}\sum_{\mathrm{j}} A_j \Big\{ \frac{3}{2}[&(d_2 - r_{2j})(-g_{1_j}^{(1)} + d_1 \times h_{11_j}^{(1)} + d_2 \times h_{12_j}^{(1)} + \\ & d_3 \times h_{13_j}^{(1)}) + (d_1 - r_{1_j})(-g_{2_j}^{(1)} + d_1 \times h_{21_j}^{(1)} + d_2 \times h_{22_j}^{(1)} + d_3 \times \\ & h_{23_j}^{(1)}) + (d_3 - r_{3_j})(-g_{1_j}^{(2)} + d_1 \times h_{11_j}^{(2)} + d_2 \times h_{12_j}^{(2)} + d_3 \times \\ & h_{13_j}^{(2)}) + (d_1 - r_{1_j})(-g_{3_j}^{(2)} + d_1 \times h_{31_j}^{(2)} + d_2 \times h_{32_j}^{(2)} + d_3 \times \\ & h_{33_j}^{(2)}) + (d_3 - r_{3_j})(-g_{2_j}^{(3)} + d_1 \times h_{21_j}^{(3)} + d_2 \times h_{22_j}^{(3)} + d_3 \times \\ & h_{23_j}^{(3)}) + (d_2 - r_{2j})(-g_{3_j}^{(3)} + d_1 \times h_{31_j}^{(3)} + d_2 \times h_{32_j}^{(3)} + d_3 \times \\ & h_{33_j}^{(3)})] + (d_1 - r_{1_j})(-g_{1_j}^{(4)} + d_1 \times h_{11_j}^{(4)} + d_2 \times h_{12_j}^{(4)} + d_3 \times \\ & h_{13_j}^{(4)}) - 2(d_2 - r_{2j})(-g_{2_j}^{(4)} + d_1 \times h_{21_j}^{(4)} + d_2 \times h_{22_j}^{(4)} + d_3 \times \\ & h_{23_j}^{(4)}) + (d_3 - r_{3_j})(-g_{3_j}^{(4)} + d_1 \times h_{31_j}^{(4)} + d_2 \times h_{32_j}^{(4)} + d_3 \times \\ & h_{33_j}^{(4)}) + (d_1 - r_{1_j})(-g_{1_j}^{(5)} + d_1 \times h_{11_j}^{(5)} + d_2 \times h_{12_j}^{(5)} + d_3 \times \\ & h_{13_j}^{(5)}) + (d_2 - r_{2_j})(-g_{2_j}^{(5)} + d_1 \times h_{21_j}^{(5)} + d_2 \times h_{22_j}^{(5)} \times d_3 \times \\ & h_{23_j}^{(5)}) - 2(d_3 - r_{3_j})(-g_{3_j}^{(5)} + d_1 \times h_{31_j}^{(5)} + d_2 \times h_{32_j}^{(5)} \times d_3 \times \\ & h_{33_j}^{(5)}) \Big\} \end{aligned} \tag{A3}$$

where $\mathbf{r}_j = \mathbf{y}_j - \mathbf{d}$ is the incenter of boundary element j in the laboratory reference frame.

Solving eq A1 for $\mathbf{d}$ is straightforward and yields

$$\begin{pmatrix} d_1 \\ d_2 \\ d_3 \end{pmatrix} = \begin{pmatrix} b_{11} & b_{12} & b_{13} \\ b_{21} & b_{22} & b_{23} \\ b_{31} & b_{32} & b_{33} \end{pmatrix}^{-1} \begin{pmatrix} c_1 \\ c_2 \\ c_3 \end{pmatrix}$$

where

$$b_{11} = \frac{1}{15}\sum_j A_j[3h_{21_j}^{(1)} + h_{31_j}^{(2)} + 2(h_{11_j}^{(4)} + h_{11_j}^{(5)})]$$

Substituting of $\mathbf{d}$ into eq 7 then gives ξ.

$$b_{12} = \frac{1}{30}\sum_j A_j[-4h_{21_j}^{(4)} + 3(h_{11_j}^{(1)} + h_{22_j}^{(1)} + h_{32_j}^{(2)} + h_{31_j}^{(3)}) + 2(h_{12_j}^{(4)} + h_{12_j}^{(5)} + h_{21_j}^{(5)})]$$

$$b_{21} = b_{12}$$

$$b_{13} = \frac{1}{30}\sum_j A_j[-4h^{(5)}_{31_j} + 3(h^{(1)}_{23_j} + h^{(2)}_{11_j} + h^{(2)}_{33_j} + h^{(3)}_{21_j}) + 2(h^{(4)}_{13_j} + h^{(4)}_{31_j} + h^{(5)}_{13_j})]$$

$$b_{22} = \frac{1}{15}\sum_j A_j(-4h^{(4)}_{22_j} + 3(h^{(1)}_{12_j} + h^{(3)}_{32_j}) + 2h^{(5)}_{22_j}))$$

$$b_{23} = \frac{1}{30}\sum_j A_j[-4(h^{(4)}_{23_j} + h^{(5)}_{32_j}) + 3(h^{(3)}_{22_j} + h^{(3)}_{33_j} + h^{(1)}_{13_j} + h^{(2)}_{12_j}) + 2(h^{(4)}_{32_j} + h^{(5)}_{23_j})]$$

$$b_{31} = b_{13}$$

$$b_{32} = b_{23}$$

$$b_{33} = \frac{1}{15}\sum_j A_j(-4h^{(5)}_{33_j} + 3(h^{(2)}_{13_j} + h^{(3)}_{23_j}) + 2h^{(4)}_{33_j}))$$

$$c_1 = \frac{1}{30}\sum_j A_j(-3g^{(1)}_{2_j} - 3g^{(2)}_{3_j} - 2g^{(4)}_{1_j} - 2g^{(5)}_{1_j} - r_{1_j}[3(h^{(1)}_{21_j} + h^{(2)}_{31_j}) + 2(h^{(4)}_{11_j} + h^{(5)}_{11_j})] - r_{2j}[3(h^{(1)}_{11_j} + h^{(3)}_{31_j}) - 4h^{(4)}_{21_j} + 2h^{(5)}_{21_j}] - r_{3_j}[3(h^{(2)}_{11_j} + h^{(3)}_{21_j}) - 4h^{(5)}_{31_j} + 2h^{(4)}_{31_j})]$$

$$c_2 = \frac{1}{30}\sum_j A_j(-3g^{(1)}_{1_j} - 3g^{(3)}_{3j} - 4g^{(4)}_{2_j} - 2g^{(5)}_{2_j} - r_{1_j}(3(h^{(1)}_{22_j} + h^{(2)}_{32_j}) + 2(h^{(4)}_{12_j} + h^{(5)}_{12_j})] - r_{2j}[3(h^{(1)}_{12_j} + h^{(3)}_{32_j}) - 4h^{(4)}_{22_j} + 2h^{(5)}_{22_j})] - r_{3_j}[3(h^{(2)}_{12_j} + h^{(3)}_{22_j}) - 4h^{(5)}_{32_j} + 2h^{(4)}_{32_j}))$$

$$c_3 = \frac{1}{30}\sum_j A_j(-3g^{(2)}_{1_j} - 3g^{(3)}_{2_j} - 2g^{(4)}_{3j} + 4g^{(5)}_{3j} - r_{1_j}[3(h^{(1)}_{23_j} + h^{(2)}_{33_j}) + 2(h^{(4)}_{13_j} + h^{(5)}_{13_j})] - r_{2j}[3(h^{(1)}_{13_j} + h^{(3)}_{33_j}) - 4h^{(4)}_{23_j} + 2h^{(5)}_{23_j}] - r_{3_j}[3(h^{(2)}_{13_j} + h^{(3)}_{23_j}) - 4h^{(5)}_{33_j} + 2h^{(4)}_{33_j})]$$

References

(1) Tanford, C.; Kawahara, K.; Lapanje, S. Proteins as random coils. I. Intrinsic viscosities and sedimentation coefficients in concentrated guanidine hydrochloride. *J. Am. Chem. Soc*. **1967**, *89*, 729−736.

(2) Morel, J.-E.; Taouil, K.; D'hahan, N.; Aguilar, A.; Merah, Z.; Dalbiez, J.-P.; Bayol, P.; Guillo, N.; Patard, L.; Cabane, V.; Ferrari, M.; Picazo, G. F.; Hieu, H. D.; Francin, M. Dimerization of native myosin LC2(RLC)-free subfragment 1 from adult rabbit skeletal muscle. *Biochemistry* **1998**, *37*, 15129−15136.

(3) Garcia de la Torre, J.; Huertas, M. L.; Carrasco, B. Calculation of Hydrodynamic Properties of Globular Proteins from Their Atomic-Level Structure. *Biophys. J.* **2000**, *78*, 719−730.

(4) Zhou, H.-X. Calculation of translational friction and intrinsic viscosity. I. General formulation for arbitrarily shaped particles. *Biophys. J.* **1995**, *69*, 2286−2297.

(5) Zhou, H.-X. Calculation of translational friction and intrinsic viscosity. II. Application to globular proteins. *Biophys. J.* **1995**, *69*, 2298−2303.

(6) Allison, S. A. The primary electroviscous effect of rigid polyions of arbitrary shape and charge distribution. *Macromolecules* **1998**, *31*, 4464−4474.

(7) Allison, S. A. Low Reynolds number transport properties of axisymmetric particles employing stick and slip boundary conditions. *Macromolecules* **1999**, *32*, 5304−5312.

(8) Aragón, S. R.; Hahn, D. K. Precise boundary element computation of protein transport properties: Diffusion tensors, specific volume, and hydration. *Biophys. J.* **2006**, in press.

(9) Wegener, W. A. On an exact starting expression for macromolecular hydrodynamic models. *Biopolymers* **1986**, *25*, 627−637.

(10) Youngren, G. K.; Acrivos, A. Stokes flow past a particle of arbitrary shape: A numerical method of solution. *J. Fluid Mech*. **1975**, *69*, 377−402.

(11) Aragon, S. R. A precise boundary element method for macromolecular transport properties. *J. Comput. Chem*. **2004**, *25*, 1191−1205.

(12) Anderson, E.; Bai, Z.; Bischof, C.; Blackford, S.; Demmel, J.; Dongarra, J.; Du Croz, J.; Greenbaum, A.; Hammarling, S.; McKenney, A.; Sorensen, D. *LAPACK Users's Guide*, 3rd ed.; SIAM: Philadelphia, PA, 1999.

(13) Simha, R. The influence of Brownian motion on the viscosity of solutions. *J. Phys. Chem*. **1940**, *44*, 25−34.

(14) Harding, S. E. The intrinsic viscosity of biological macromolecules. Progress in measurement, interpretation and application to structure in dilute solution. *Prog. Biophys. Mol. Biol*. **1997**, *68*, 207−262.

(15) Madeley, C. R.; Field, A. M. *Virus Morphology*, 2nd ed.; Churchill Livingstone: New York, 1988.

(16) Garcia de la Torre, J.; Bloomfield, V. A. Hydrodynamic properties of macromolecular complexes. IV. Intrinsic viscosity, with application to once-broken rods and multisubunit proteins. *Biopolymers* **1978**, *17*, 1605−1627.

(17) Einstein, A. Berichtigung zu meiner Arbeit: "Eine neue Bestimmung der Molekulardimensionen". *Ann. Phys*. **1911**, *34*, 591−597.

(18) Connolly, M. L. Analytical molecular surface calculation. *J. Appl. Crystallogr*. **1983**, *16*, 548−558.

(19) Shoemaker, D. P.; Garland, C. W.; Nibler, J. W. *Experiments in Physical Chemistry*, 5th ed.; McGraw-Hill: New York, 1989.

(20) Monkos, K. Viscometric study of human, bovine, equine and ovine haemoglobin in aqueous solution. *Int. J. Biol. Macromol*. **1994**, *16*, 31−35.

(21) Quershi, S. H.; Moza, B.; Yadav, S.; Ahmad, F. Configurational and thermodynamic characterization of the molten globule state occurring during unfolding of cytochrome-c by weak salt. *Biochemistry* **2003**, *42*, 1684−1695.

(22) Fling, M.; Horowitz, N. H.; Heinemann, S. F. The isolation and properties of crystalline tyrosinase from neurospora. *J. Biol. Chem*. **1963**, *238*, 2045−2053.

(23) Larew, L.; Walters, R. W. A kinetic, chromatographic method for studying protein hydrodynamic behavior. *Anal. Biochem*. **1987**, *164*, 537−546.

(24) Walters, R. W.; Graham, J. F.; Moore, R. M.; Anderson, D. J. Protein diffusion coefficient measurements by laminar flow analysis: Method and applications. *Anal. Biochem.* **1984**, *140*, 190−195.

(25) Clark, S. M.; Leaist, D. G.; Konermann, L. Taylor dispersion monitored by electrospray mass spectrometry: A novel approach for studying diffusion in solution. *Rapid Commun. Mass Spectrom*. **2002**, *16*, 1454−1462. Converted from $D_t = 13.5$ cm^2/s at 24 °C.

(26) Buzzell, J. G.; Tanford, C. The effect of charge and ionic strength on the viscosity of ribonuclease. *J. Phys. Chem*. **1956**, *60*, 1204−1207.

(27) Kupke, D. W.; Hodgkins, M. G.; Beams, J. W. Simultaneous determination of viscosity and density of protein solutions by magnetic suspension. *Proc. Natl. Acad. Sci. U.S.A.* **1972**, *69*, 2258−2262.

(28) Creeth, J. M. Studies of free diffusion in liquids with the Rayleigh method. III. The analysis of known mixtures and some preliminary investigations with proteins. *J. Phys. Chem.* **1958**, *62*, 66−74. Converted from $D_t = 12.11$ cm^2/s at 25 °C.

(29) Wetlaufer, D. B. Osmometry and general characterization of alpha-lactalbumin. *C. R. Trav. Lab. Carlsberg* **1961**, *32*, 125−138.

(30) Dolgikh, D. A.; Gilmanshin, R. I.; Braznikov, E. V.; Bychkova, V. E.; Semisotnov, G. V.; Venyaminov, S. Y.; Ptitsyn, O. B. Alpha-lactalbumin: Compact state with fluctuating tertiary structure. *FEBS Lett.* **1981**, *136*, 311−315.

(31) Polson, A. Über die berechnung der gestalt von proteinmolekülen. *Kolloid Z.* **1939**, *88*, 51−61.

(32) Gordon, W. G.; Semmett, W. F. Isolation of crystalline α-lactalbumin from milk. *J. Am. Chem. Soc*. **1953**, *75*, 328−330.

(33) Monkos, K. Concentration and temperature dependence of viscosity in lysozyme aqueous solutions. *Biochim. Biophys. Acta* **1997**, *1339*, 304−310.

(34) Kamiyama, T.; Morita, M.; Kimura, T. Rheological study of lysozyme in dimethyl sulfoxide + water solution at 298.15 K. *J. Chem. Eng. Data* **2004**, *49*, 1350−1353.

(35) Luzzati, A.; Champagne, M. The molecular weight and dimensions of the lysozyme molecule in solution. *C. R. Hebd. Seances Acad. Sci.* **1957**, *244*, 2930−2932.

(36) Sophianopoulos, A. J.; Rhodes, C. K.; Holcomb, D. N.; van Holde, K. E. Physical studies of lysozyme. I. Characterization. *J. Biol. Chem*. **1962**, *237*, 1107−1112.

(37) Bouthier, M.; Quaranta, C.; Savary, J.; Reynaud, J. Détermination du nombre de viscosité limite des proteins. Application aux anhydrases carboniques erythrocytaires humaines. *J. Chim. Phys. Phys.-Chim. Biol.* **1976**, *73*, 776−782.

(38) Dubin, S. B.; Clark, N. A.; Benedek, G. B. Measurements of the rotational diffusion coefficient of lysozyme by depolarized light scattering. I. Configuration of lysozyme in solution. *J. Chem. Phys*. **1971**, *54*, 5158−5164.

(39) Harding, S. E. Viscometric parameters for myoglobin. *IRCS Med. Sci.* **1980**, *8*, 610.

(40) Ehrenberg, A. Determination of molecular weights and diffusion coefficients in the ultracentrifuge. *Acta Chem. Scand*. **1957**, *11*, 1257−1270.

(41) Riveros-Moreno, V.; Wittenberg, J. B. The self-diffusion coefficients of myoglobin and hemoglobin in concentrated solutions. *J. Biol. Chem*. **1972**, *247*, 895−901.

(42) Edelhoch, H.; Steiner, R. F. Structural transitions of soybean trypsin inhibitor. II. The denatured state in urea. *J. Biol. Chem.* **1963**, *238*, 931−938.

(43) Rackis, J. J.; Sasame, H. A.; Mann, R. K.; Anderson, R. L.; Smith, A. K. Soybean trypsin inhibitors: Isolation, purification and physical properties. *Arch. Biochem. Biophys.* **1962**, *98*, 471−478. Calculated from the Svedberg equation using $s_{20,w} = 2.29$ S and $\bar{\nu} = 0.735$ cm^3/g and assuming solvent density $\rho = 1.0$ g/cm^3.

(44) Harris, J. L. Effect of urea on trypsin and alpha-chymotrypsin. *Nature* **1956**, *177*, 471−473.

(45) Cunningham, L. W., Jr.; Tietze, F.; Green, N. M.; Neurath, H. Molecular kinetic properties of trypsin and related proteins. *Discuss. Faraday Soc.* **1953**, *13*, 58−67.

(46) Kay, C. M.; Smillie, L. B.; Hilderman, F. A. The molecular weight of trypsinogen. *J. Biol. Chem.* **1961**, *236*, 118−121.

(47) Tietze, F. Molecular-kinetic properties of crystalline trypsinogen. *J. Biol. Chem.* **1953**, *204*, 1−11.

(48) Schwert, G. W.; Kaufman, S. The molecular size and shape of the pancreatic proteases. III. α-chymotrypsin. *J. Biol. Chem.* **1951**, *190*, 807−816.

(49) Tanford, C. Protein denaturation. *Adv. Protein Chem.* **1968**, *23*, 121−282.

(50) Schwert, G. W. The molecular size and shape of the pancreatic proteases. II. Chymotrypsinogen. *J. Biol. Chem.* **1951**, *190*, 799−806. Calculated from $[\eta] = \xi\bar{\nu}$, where ξ is the viscosity factor and $\bar{\nu}$ is the partial molar volume.

(51) Wilcox, P. E.; Kraut, J.; Wade, R. D.; Neurath, H. The molecular weight of alpha-chymotrypsinogen. *Biochim. Biophys. Acta* **1957**, *24*, 72−78.

(52) Armstrong, J. M.; Myers, D. V.; Verpoorte, J. A.; Edsall, J. T. Purification and properties of human erythrocite carbonic anhydrases. *J. Biol. Chem.* **1966**, *241*, 5137−5149.

(53) Wong, K.-P.; Tanford, C. Denaturation of bovine carbonic anhydrase b by guanidine hydrochloride. A process involving sequential conformational transitions. *J. Biol. Chem.* **1973**, *248*, 8518−8523.

(54) Bürgi, W.; Schmid, K. Preparation and properties of Zn-alpha2-glycoprotein of normal human plasma. *J. Biol. Chem.* **1961**, *236*, 1066−1074. Calculated from the Svedberg equation using $s_{20,w} = 3.1$ S and $\bar{\nu} = 0.706$ cm^3/g and assuming solvent density $\rho = 1.0$ g/cm^3.

(55) Blumenfeld, O. O.; Léonis, J.; Perlmann, G. E. The effect of guanidine hydrochloride on crystalline pepsin. *J. Biol. Chem.* **1960**, *235*, 379−382.

(56) Edelhoch, H. The denaturation of pepsin. I. Macromolecular change. *J. Am. Chem. Soc.* **1957**, *79*, 6100−6109.

(57) Neurath, H.; Cooper, G. R.; Erickson, J. O. The shape of protein molecules. II. Viscosity and diffusion studies of native proteins. *J. Biol. Chem.* **1941**, *138*, 411−436.

(58) Cohen, L. B. Viscosity of g-ADP and g-ATP actin. *Arch. Biochem. Biophys.* **1966**, *117*, 289−295.

(59) Lanni, F.; Ware, B. R. Detection and characterization of actin monomers, oligomers, and filaments in solution by measurement of fluorescence photobleaching recovery. *Biophys. J.* **1984**, *46*, 97−110.

(60) Newman, J.; Estes, J. E.; Selden, L. A.; Gershman, L. C. The presence of oligomers at subcritical actin concentrations. *Biochemistry* **1985**, *24*, 1538−1544.

(61) Takagi, T.; Isemura, T. Extent of renaturation of reduced taka-amylase a before reformation of disulfide bonds. *Biochim. Biophys. Acta* **1966**, *130*, 233−240.

(62) Isemura, T.; Fujita, S. Physicochemical studies on taka-amylase a. I. Size and shape determination by the measurement of sedimentation constant, diffusion constant, and viscosity. *J. Biochem. (Tokyo)* **1957**, *44*, 443−450.

(63) Muzammil, S.; Kumar, Y.; Tayyab, S. Molten globule-like state of human serum albumin at low pH. *Eur. J. Biochem.* **1999**, *266*, 26−32.

(64) Oncley, J. L.; Scatchard, G.; Brown, A. Physical-chemical characteristics of certain of the proteins of normal human plasma. *J. Phys. Colloid Chem.* **1947**, *51*, 184−198.

(65) Monkos, K. On the hydrodynamics and temperature dependence of the solution conformation of human serum albumin from viscometry approach. *Biochim. Biophys. Acta* **2004**, *1700*, 27−34.

(66) Pedersen, K, O. *Ultracentrifugal Studies on Serum and Serum Fractions*; Almqvist and Wiksells: Upsala, 1945.

(67) Charlwood, P. A. Sedimentation and diffusion of human albumins. I. Normal human albumins at low concentration. *Biochem. J.* **1952**, *51*, 113−118.

(68) Phelps, R. A.; Cann, J. R. On the modification of conalbumin by acid. II. Effect of pH and salt concentration on the sedimentation behavior, viscosity and osmotic pressure of conalbumin solutions. *Arch. Biochem. Biophys.* **1956**, *61*, 51−71.

(69) Yajima, H.; Yamamoto, H.; Nagaoka, M.; Nakazato, K.; Ishii, T.; Niimura, N. Small-angle neutron scattering and dynamic light scattering studies of N- and C-terminal fragments of ovotransferrin. *Biochim. Biophys. Acta* **1998**, *1381*, 68−76. Converted from $D_t = 6.7 \times 10^{-7}$ cm^2/s at 25 °C.

(70) Léger, D.; Verbert, A.; Loucheux, M.-H.; Spik, G. Etude de la moléculaire de la lactotransferrine et de la serotransferrine humaines. *Ann. Biol. Anim. Biochem. Biophys.* **1977**, *17*, 737−747.

(71) Querinjean, P.; Masson, P. L.; Heremans, J. F. Molecular weight, single-chain structure and amino acid composition of human lactoferrin. *Eur. J. Biochem.* **1971**, *20*, 420−425.

(72) Wood, E.; Dalgleish, D.; Bannister, W. Bovine erythrocite cupro-zinc protein. 2. Physicochemical properties and circular dichroism. *Eur. J. Biochem.* **1971**, *18*, 187−193.

(73) Bunville, L. G. Ph.D. Thesis, Iowa State University, 1959.

(74) McKenzie, H. A.; Sawyer, W. H. Effect of pH on β-lactoglobulin. *Nature* **1967**, *214*, 1101−1104.

(75) Bull, H. B.; Currie, B. T. Osmotic pressure of β-lactoglobulin solutions. *J. Am. Chem. Soc.* **1946**, *68*, 742−745.

(76) Fox, K. K.; Holsinger, V. H.; Posati, L. P.; Pallansch, M. J. Separation of beta-lactoglobulin from other milk serum proteins by trichloroacetic acid. *J. Dairy Sci.* **1967**, *50*, 1363−1367.

(77) Ogston, A. G. The Guoy diffusiometer; further calibration. *Proc. R. Soc. London* **1949**, *196*, 272−285.

(78) Samsonov, G. V.; Ponomareva, R. B.; Bolotina, I. A. Investigation of the physical-chemical properties of α-chymotrypsin and its B and C chain. *Biofizika* **1965**, *10*, 520−522.

(79) Schwert, G. W.; Kaufman, S. The molecular size and shape of the pancreatic proteases. III. α-Chymotrypsin. *J. Biol. Chem.* **1951**, *190*, 807−816.

(80) Kunitz, M.; Northrop, J. H. Crystalline chymo-trypsin and chymo-trypsinogen: I. Isolation, crystallization, and general properties of a new proteolytic enzyme and its precursor. *J. Gen. Physiol.* **1935**, *18*, 433−458.

(81) McCubbin, W. D.; Kay, C. M. Molecular weight studies on concanavalin A. *Biochem. Biophys. Res. Commun.* **1971**, *44*, 101−109.

(82) Huet, M.; Claverie, J.-M. Sedimentation studies of the reversible dimer−tetramer transition kinetics of concanavalin A. *Biochemistry* **1978**, *17*, 236−241.

(83) McVittie, J. D.; Esnouf, M. P.; Peacocke, A. R. The denaturation of chicken-muscle triosephosphate isomerase in guanidinium chloride. *Eur. J. Biochem.* **1977**, *81*, 307−315. D_t calculated from the Svedberg equation using $s_{20,w} = 3.75$ S and $\bar{\nu} = 0.740$ cm^3/g and assuming solvent density $\rho = 1.0$ g/cm^3.

(84) Frénoy, J.-P. Effect of physical environment on the conformation of ricin. Influence of low pH. *Biochem. J.* **1986**, *240*, 221−226.

(85) Kabat, E. A.; Heidelberger, M.; Bezer, A. E. A study of the purification and properties of ricin. *J. Biol. Chem.* **1947**, *168*, 629−639.

(86) Sanders, A. H.; Purich, D. L.; Cannell, D. S. Oxygenation of hemoglobin: Correspondence of crystal and solution properties using translational diffusion constant measurements. *J. Mol. Biol.* **1981**, *147*, 583−595.

(87) Reynolds, J. A.; Schlesinger, M. J. Conformational states of the subunit of *Escherichia coli* alkaline phosphatase. *Biochemistry* **1967**, *6*, 3552−3559.

(88) Altman, P. L.; Dittmer, D. S. *Biology Data Book*, 2nd ed.; FASEB: Bethesda, Maryland, 1972; Vol. I. Calculated from the Svedberg equation using $s_{20,w} = 6.1$ S and $\bar{\nu} = 0.725$ cm^3/g and assuming solvent density $\rho = 1.0$ g/cm^3.

(89) Wu, J.-Y.; Yang, J. T. Physicochemical characterization of citrate synthase. *J. Biol. Chem.* **1970**, *24*, 212−218.

(90) Wong, S. C. K.; Hall, D. C.; Josse, J. Constitutive inorganic pyrophosphatase of *Escherichia coli*. III. Molecular weight and physical properties of the enzyme and its subunits. *J. Biol. Chem.* **1970**, *245*, 4335−4341.

(91) Castellino, J.; Barker, R. Examination of the dissociation of multichain proteins in guanidine hydrochloride by membrane osmometry. *Biochemistry* **1968**, *7*, 2207−2217.

(92) Stellwagen, E.; Schachman, H. K. The dissociation and reconstitution of aldolase. *Biochemistry* **1962**, *1*, 1056−1069.

(93) Hass, L. F. Aldolase dissociation into subunits by reaction with succinic anhydride. *Biochemistry* **1964**, *3*, 535−541.

(94) Glikina, M. V.; Finogenov, P. A. Investigation of muscular aldolase in various stages of isolation. *Biokhimiya* **1950**, *15*, 457−464.

(95) Kawahara, K. Evaluation of diffusion coefficients of proteins from sedimentation boundary curves. *Biochemistry* **1969**, *8*, 2551−2557.

(96) Taylor, J. F.; Green, A. A.; Cori, G. T. Crystalline aldolase. *J. Biol. Chem.* **1948**, *173*, 591−604.

(97) Christen, P.; Göschke, H.; Leuthardt, F.; Schmid, A. Über die aldolase der kaninchenleber molekulargewicht, dissoziation in untereinheiten. *Helv. Chim. Acta* **1965**, *48*, 1050−1056.

(98) Tanford, C.; Lovrien, R. Dissociation of catalase into subunits. *J. Am. Chem. Soc.* **1962**, *84*, 1892−1896.

(99) Samejima, T.; Yang, J. T. Reconstitution of acid-denatured catalase. *J. Biol. Chem.* **1963**, *238*, 3256−3261.

(100) Sumner, J.; Gralén, N. The molecular weight of crystalline catalase. *Science* **1938**, *87*, 284.

(101) Samejima, T. Splitting of the catalase molecule by alkali treatment. *J. Biochem.* **1959**, *46*, 155−159.

(102) Sund, H.; Weber, K. Studies on the lactose-splitting enzyme. XIII. Quantity and configuration of beta-galactosidase from *E. coli*. *Biochem. Z.* **1963**, *363*, 24−34.

(103) Tellam, R.; Winzor, D. J. Self-association of alpha-chymotrypsin at low ionic strength in the vicinity of its pH optimum. *Biochem. J.* **1977**, *161*, 687−694.

(104) McEvily, A. J.; Harrison, J. H. Subunit equilibria of porcine heart citrate synthase. Effects of enzyme concentration, pH, and substrates. *J. Biol. Chem.* **1986**, *261*, 2593−2598.

(105) Avaeva, S.; Grigorjeva, D.; Mitkevich, V.; Sklyankina, V.; Varfolomeyev, S. Interaction of *Escherichia coli* inorganic pyrophosphatase active sites. *FEBS Lett.* **1999**, *464*, 169−173.

(106) Malinowski, D. P.; Fridovich, I. Subunit association and side-chain reactivities of bovine erythrocyte superoxide dismutase in denaturing solvents. *Biochemistry* **1979**, *18*, 5055−5060.

(107) Lebherz, H. G. Stability of quaternary structure of mammalian and avian fructose diphosphate aldolases. *Biochemistry* **1972**, *11*, 2243−2250.

(108) Senear, D. F.; Teller, D. C. Thermodynamics of concanavalin a dimer−tetramer self-association: Sedimentation equilibrium studies. *Biochemistry* **1981**, *20*, 3076−3083.

(109) Garen, A.; Levinthal, C. A fine-structure genetic and chemical study of the enzyme alkaline phosphatase of *E. coli*. I. Purification and characterization of alkaline phosphatase. *Biochim. Biophys. Acta* **1960**, *38*, 470−483.

(110) Borchert, T. V.; Abagyan, R.; Jaenicke, R.; Wierenga, R. K. Design, creation, and characterization of a stable, monomeric triosephosphate isomerase. *Proc. Natl. Acad. Sci. U.S.A.* **1994**, *91*, 1515−1518.

(111) Chiancone, E.; Gilbert, L. M.; Gilbert, G. A.; Kellett, G. L. Dissociation of hemoglobin into subunits. II. Human oxyhemoglobin: Gel filtration studies. *J. Biol. Chem.* **1968**, *243*, 1212−1219.

(112) Lukin, J. A.; Kontaxis, G.; Simplaceanu, V.; Yuan, Y.; Bax, A.; Ho, C. Quaternary structure of hemoglobin in solution. *Proc. Natl. Acad. Sci. U.S.A.* **2003**, *100*, 517−520.

(113) Silva, M. M.; Rogers, P. H.; Arnone, A. A third quaternary structure of human hemoglobin A at 1.7-Å resolution. *J. Biol. Chem.* **1992**, *267*, 17248−17256.

(114) Rutenber, E.; Katzin, B. J.; Montfort, W.; Villafranca, J. E.; Ernst, S.; Collins, E. J.; Mlsna, D.; Ready, M. P.; Robertus, J. D. Crystallographic refinement of ricin to 2.5 Å. *Proteins: Struct., Funct., Genet.* **1991**, *10*, 240−250.

(115) Bushnell, G. W.; Louie, G. V.; Brayer, G. D. High-resolution structure of horse heart cytochrome C. *J. Mol. Biol.* **1990**, *214*, 585−595.

(116) Sweeney, E. C.; Tonevitsky, A. G.; Temiakov, D. E.; Agapov, I. I.; Saward, S.; Palmer, R. A. Preliminary crystallographic characterization of ricin agglutinin. *Proteins* **1997**, *28*, 586−589.

CT600062Y